Stem Cell Research & Therapy

RESEARCH

Open Access

A chitosan/acellular matrix-based neural graft carrying mesenchymal stem cells to promote peripheral nerve repair

Zhifa Zhang[1], Molin Li[2,3], Gang Cheng[1], Peng Wang[1], Chunhui Zhou[4], Yang Liu[5], Xiaofeng Duan[6], Jing Wang[7], Fang Xie[3*], Yaqiong Zhu[3*] and Jianning Zhang[1*]

Abstract

Background Treatment of peripheral nerve defects is a major concern in regenerative medicine. This study therefore aimed to explore the efficacy of a neural graft constructed using adipose mesenchymal stem cells (ADSC), acellular microtissues (MTs), and chitosan in the treatment of peripheral nerve defects.

Methods Stem cell therapy with acellular MTs provided a suitable microenvironment for axonal regeneration, and compensated for the lack of repair cells in the neural ducts of male 8-week-old Sprague Dawley rats.

Results In vitro, acellular MTs retained the intrinsic extracellular matrix and improved the narrow microstructure of acellular nerves, thereby enhancing cell functionality. In vivo neuroelectrophysiological studies, gait analysis, and sciatic nerve histology demonstrated the regenerative effects of active acellular MT. The Chitosan + Acellular-MT + ADSC group exhibited superior myelin sheath quality and improved neurological and motor function recovery.

Conclusions Active acellular-MTs precellularized with ADSC hold promise as a safe and effective clinical treatment method for peripheral nerve defects.

Keywords Peripheral nerve injury, Mesenchymal stem cells, Tissue repair, Biomaterials, Chitosan, Acellular nerve

[†]Zhifa Zhang, Molin Li and Gang Cheng have contributed equally to this work.

*Correspondence:
Fang Xie
lmsh1225@163.com
Yaqiong Zhu
zhuyaqiong28@163.com
Jianning Zhang
zhangjianning301@sina.com
Full list of author information is available at the end of the article

Graphical abstract

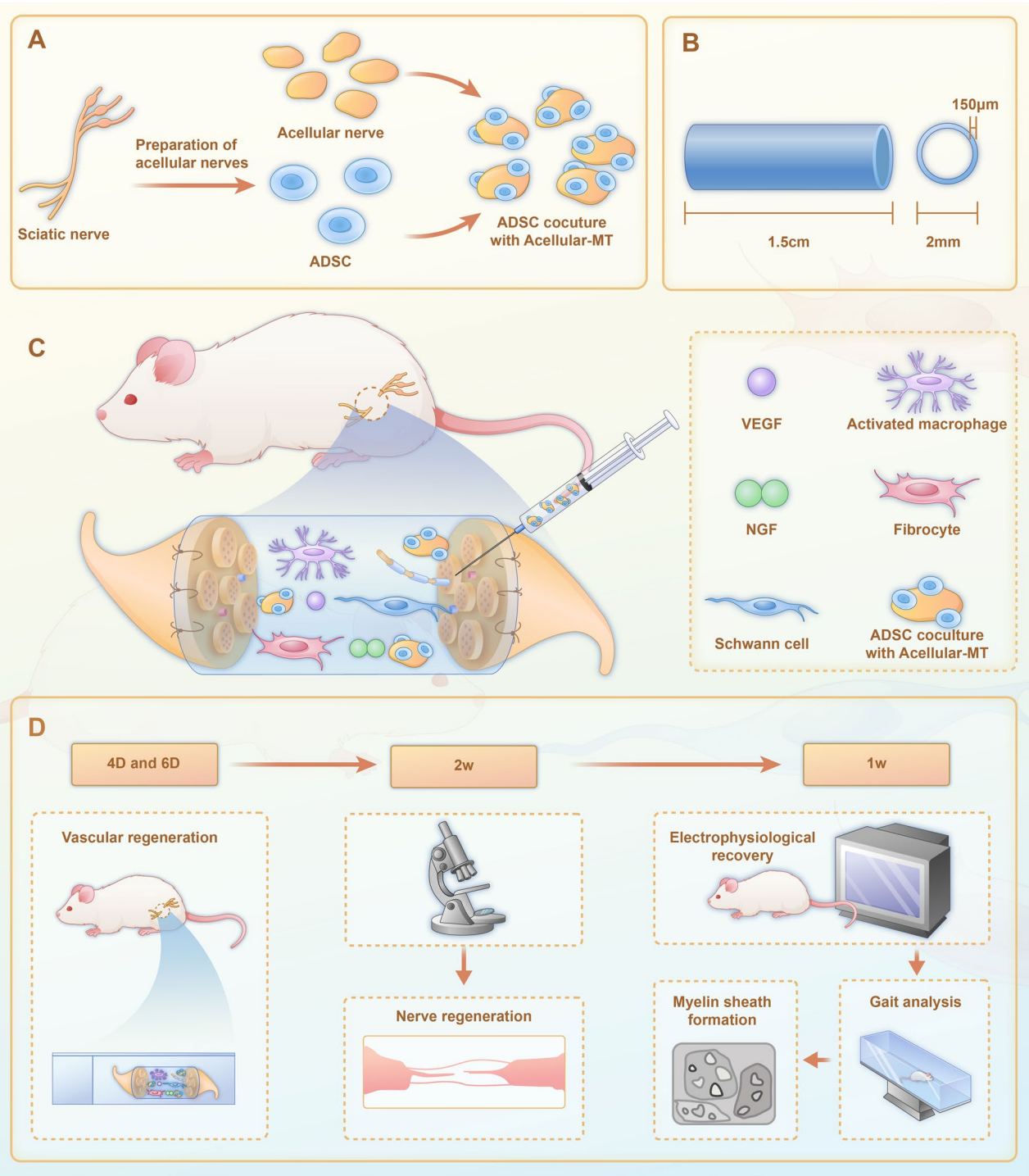

Background

Peripheral nerve injuries are common. However, owing to the slow regeneration rate of axons, the target muscle after nerve injury faces long-term denervation, causing irreversible damage [1, 2]. Severe nerve deficits are often accompanied by long nerve spaces that do not heal

spontaneously; thus, bridging grafts are often required to accelerate axon regeneration [3]. Several advances have been made in nerve graft scaffolds, including the use of abundant natural biomaterials, synthetic materials, and autografts. These scaffolds have good biocompatibility, suitable degradation cycles, and tensile strength, and are suitable for different degrees of peripheral nerve defect repair [4–7]. Acellular nerve allografts (ANA) are an alternative to autografts. Numerous studies have suggested that ANA combined with cell or molecular therapy holds promise for nerve regeneration [8]. After nerve injury, endogenous Schwann cells have limited repair functions, particularly in acellular nerve grafts with long nerve defects (> 3 cm) [7, 9]. Stem cell therapy can accelerate axon regeneration and help neurons survive, and has shown significant advantages in the repair of peripheral nerve defects [10]. Adipose-derived mesenchymal stem cells (ADSCs) promote tissue regeneration by releasing active factors. ADSCs have the potential for self-renewal and multidirectional differentiation, and are readily available and expanded in vitro, making them one of the best cells for combination therapy with acellular nerves [11, 12].

Important components of acellular nerves, such as the intrinsic extracellular matrix (ECM) and complex microstructure [13], can recruit Schwann cells to migrate from the stump of the nerve defect to the interior of the nerve graft to induce neurotrophic factors and other biologically active substances [3, 14]. Injured axons regenerate and extend to the distal end of the graft [15]. As such, preserving an intact ECM structure is key to promoting axon regeneration [16]. However, the internal structure of normal acellular nerves is very dense, making it difficult for the regenerated axons to span the graft. In addition, the degree of control of the cell-free chemical processes affects their clinical application. Although existing decellularization methods have been shown to decellularize well, there still have some shortcomings in preserving relatively abundant ECM components, such as laminin and fibronectin [17]. Conversely, preserving more ECM or the dense structure of normal acellular nerves may result in insufficient immunogenic clearance. However, excessive detergent residue can spread to the connection between the graft and nerve endings, which is potentially dangerous for transplantation treatment [6, 8, 18].

In the present study, we constructed acellular nerve microtissues (MTs) with an appropriate degree of decellularization and a large-pore structure to promote the growth of regenerated myelinated nerves with low immunogenicity and biotoxicity. The standard decellularization process was performed after the nerves were prepared into 1 mm microparticles. Combining ADSCs with acellular microparticles to construct MT, and using chitosan as a scaffold could simulate the construction of a three-dimensional culture dish suitable for promoting the survival of a large number of cells and providing ADSCs with delivery functions, such as targeting the damaged site to release bioactive molecules.

Materials and methods

Culture and treatment of adipose mesenchymal stem cells

ADSCs were extracted from SD rats by accepted protocols [19]. All animal experiments in this study were performed in accordance with the guidelines and regulations related to the care and use of laboratory animals presented by the Animal Ethics Committee of the Chinese PLA General Hospital (Code No. 2022-X18-37). Fat pad tissues were acquired from 4 to 6-week-old SD rats were anesthetization by isoflurane inhalation. The fat pad tissues were then carefully rinsed using Hank's balanced salt solution. Subsequently, the tissues were minced and the fragments were digested using collagenase type I (2 mg/ml; Biochrom, Berlin, Germany) and shaken at 37 °C for 60 min. The cell pellet was then centrifuged at 620×*g* for 10 min, and resuspended in ADSC Dulbecco's Modified Eagle Medium (DMEM)/F12 (Biochrom) with 100 U/ml penicillin, 100 mg/ml streptomycin (P/S; PAA), 0.2 mM L-ascorbic acid-2-phosphate (A2P; Sigma), and 10% fetal bovine serum (FBS; Biochrom). ADSCs were incubated at 37 °C, 5% CO_2 environment, and the medium was changed after 2–3 days. Immunofluorescence staining was applied to identify CD44 (Abcam, ab238464) expression on the surface of ADSCs. The osteogenic and adipogenic differentiation capacities of ADSCs were verified, and surface antigens were identified using flow cytometry.

Preparation of acellular nerves

The study protocol was approved and supervised by the Ethics Committee of the Chinese People's Liberation Army General Hospital (2022-X18-37). Acellular nerves were prepared from 30 male Sprague–Dawley rats (8 weeks old) weighing 200–250 g. The sciatic nerve segment, extending approximately 20 mm from the hind limb, was excised under aseptic conditions with 1% pentobarbital sodium anesthesia. Blood, peripheral fat, and connective tissue around the sciatic nerve were carefully removed, and the dissected sciatic nerves were stored in precooled phosphate buffered saline at 4 °C. The nerves were then cut into pieces for further use. To prepare the acellular nerves, nerve segments were soaked in distilled water for 7 h, 3.0% (5v/v) Triton X-100 (Sigma-Aldrich, USA) treated for 12 h, distilled water three times for 15 min, 4.0% (w/v) sodium deoxycholate (Sigma-Aldrich, USA) for 12 h, and distilled water three times

for 15 min. All operations were performed with stirring at room temperature (120 rpm) [20, 21]. All animals were sacrificed under inhalation isoflurane anesthesia after the experiments.

HE staining and immunostaining of nerves

Normal sciatic and acellular nerves were fixed in 4% PFA for 24 h. For the treatment of the rat tissue, grafts of 1 cm were obtained from each group. The two nerves were fixed in 4% PFA for 16 h and embedded in paraffin. Sections (5 μm) were obtained on poly-lysine-adhesive slides, and blocked with 10% goat serum for 2 h. Immunostaining was performed following previously accepted protocols. The sections were incubated overnight at 4 °C with primary antibodies, after which slides were stained with secondary antibodies. Nuclei were stained with DAPI.

At 4 and 6 days postoperatively, 6 μm longitudinal sections of the nerve graft segments were collected in each group to evaluate myelin regeneration and vascular endothelial reconstruction. Immunofluorescence staining was performed for each group, using rabbit anti-S100 (Abcam, ab34686) or mouse anti-REGA-1 (Abcam, ab22492) as the primary antibody and one of the following secondary antibodies: donkey anti-rabbit IgG H&L (Alexa Fluor®488, Abcam, ab150073), goat anti-mouse IgG H&L (Alexa Fluor®647, Abcam, ab150115). The remaining steps were the same as those described above.

Live/dead cell staining

After coincubating the acellular neural microparticles with ADSCs for 48 h, the toxic effects of the acellular nerves on ADSC were evaluated using live/dead cell staining. Cells were incubated for 15 min with fluorescein diacetate (FDA) and propidium iodide (PI), which stained live and dead cells. respectively. Fluorescence images were captured using an electron microscope (Hitachi H7500; Tokyo, Japan) to determine the ratio of cell death to survival.

Nerve defect animal model

All procedures described in this study were approved by the Ethics Committee of Chinese PLA General Hospital (SQ2022437). All animals were sacrificed under inhaled isoflurane anesthesia after the experiments. All 48 male 8-week-old Sprague Dawley rats (weight 200–250 g) were maintained under a 12:12 h light/dark cycle. Sample sizes were calculated using the Power Analysis and Sample Size (PASS) software (version 11.0; NCSS, USA) based on pre-experimental results. The animals were randomly assigned to four groups (n = 5) according to the bridging graft at the nerve defect, as follows: chitosan, chitosan + cellular-MT, chitosan + cellular-MT + ADSC, and autografts. Animals were anesthetized through an intraperitoneal injection of 2% sodium pentobarbital. A rat model of sciatic nerve defects in the right hindlimb was constructed. After dehairing the right hind limb, the skin was incised, and the sciatic nerve was exposed and bluntly separated. A 10 mm long sciatic nerve was excised from the midthigh, and a 10 mm long gap was created. In the chitosan group, the chitosan conduit was sutured to both ends of the sciatic nerve defect. In the Chitosan + Acellular-MT and Chitosan + Acellular-MT + ADSC groups, chitosan with an appropriate amount of acellular microparticles was carefully stitched into the nerve stump. For the Chitosan + Acellular-MT + ADSC group, additional ADSCs were injected into chitosan with preplaced acellular microparticles. In the autograft group, the 10 mm sciatic nerve was reversed and sutured to both ends of the nerve stump. All surgeries were performed under sterile conditions using 8–0 nylon sutures. The skin and muscles were sequentially sutured using 5–0 nylon sutures. All animals were housed in animal houses under standard conditions (Temperature 19–22 °C, humidity 40–50%, 12:12 h light and dark cycle).

Flow cytometry

The surface antigens of ADSCs were identified using flow cytometry. In brief, cells were incubated with specific antibodies for 30 min at room temperature according to accepted protocols, washed twice with PBS, and resuspended in 500 uL of PBS. Primary antibodies included anti-CD45 (Abcam, ab40763), anti-CD31 (Abcam, ab28364), anti-CD90 (Abcam, ab92574), and anti-CD29 (GTX112971), and cell percentages were analyzed using FlowJo software (Tri Star Inc., Ashland, USA).

Gait analysis

Footprint analysis was performed on all rats to assess the recovery of motor function at 4-, 8-, and 12- weeks (W) after treatment. The test used a one-way channel with sidewalls and a white strip placed at the bottom to record the footprint of the rat. The rats were tested under specific conditions by prompting them to move in one direction along the track, and ink-treated rat footprints were recorded on the strips. At least three pairs of footprints were recorded for each rat, and the sciatic nerve function index (SFI) was calculated. The sciatic nerve function index was calculated using the following formula:

$$\mathbf{SFI} = \left(\left(\frac{(\mathbf{ETOF} - \mathbf{NTOF})}{\mathbf{NTOF}}\right) + \left(\frac{(\mathbf{NPL} - \mathbf{EPL})}{\mathbf{EPL}}\right) + \left(\frac{(\mathbf{ETS} - \mathbf{NTS})}{\mathbf{NTS}}\right) + \left(\frac{(\mathbf{EIT} - \mathbf{NIT})}{\mathbf{NIT}}\right) \times \frac{220}{4}$$

The treatment effect was assessed by analyzing the walking trajectories of the rats on the experimental and control side. The following parameters were measured: distance between the footprints (TOF), print length (PL), distance from the heel to the third toe, toe spread (TS), distance from the first toe to the fifth toe, intermediary toe spread (IT), and distance between the second toe and fourth toes; E, experimental group; N, normal group. Simultaneously, the standing/swing time ratio (injured side/normal side) was calculated.

Nerve conduction studies

To assess sciatic nerve conduction before and at 8 W post-treatment, the compound muscle action potentials (CMAPs) were measured in all rats using an MG-42 Tendonograph (Hungary). After the rats were anesthetized, monopolar needle electrodes were inserted into the hip joint and the sciatic nerve area was continuously stimulated with square-wave pulses. The stimulation time was 1–2 ms, and the intensity was 3.0 mA, 1.0 Hz. The cathode of the monopolar needle electrode was inserted into the belly of the medial gastrocnemius muscle, while the anode was inserted into the tendon. The latency, threshold, duration, and maximum potential amplitude of the CMAPs were recorded and analyzed.

Scanning electron microscope characterization

The morphological features of normal nerves, acellular nerves, and chitosan were all assessed by scanning electron microscopy (SEM). Simultaneously, the distal nerves of the grafted rats were examined by transmission electron microscopy at 12 W postoperatively to observe the morphology of axons and myelin sheath recovery. All samples were fixed in 2.5% glutaraldehyde for 24 h, and the morphology was observed using a transmission electron microscope (CM-120, PHILIPS, Netherlands).

Statistical analysis

All data were expressed as the mean ± standard deviation. GraphPad Prism9 and the Statistical Program for Social Sciences (SPSS) software (version 22.0) were used for statistical analyses. The normal distribution of the data was evaluated using the Kolmogorov–Smirnov test. One-way analysis of variance (ANOVA) was applied to analyze and compare data between multiple groups, and a P value < 0.05 indicated that the data were statistically different. All representative data were analyzed from at least three independent experiments.

The work was reported in line with the ARRIVE guidelines 2.0.

Results

Isolation and culture of ADSC

ADSCs were extracted from rat fat pads and identified. ADSCs showed obvious cobblestone morphology and had the potential for multilineage differentiation. Calcium deposition was observed during osteogenic differentiation, while lipid droplets were observed in the cytoplasm during adipose-induced differentiation. These were identified using Alizarin Red S and Oil Red O staining. In addition, flow cytometry was applied to identify cell surface markers. The results showed that the extracted ADSCs highly expressed CD90 and CD29, but did not express CD31 and CD45. These results indicate that the extracted ADSC conformed to the characteristics of typical ADSC. (Fig. 1).

Morphology of chitosan under transmission electron microscope and evaluation of acellular nerve microstructure and pore size

The microstructural morphology of the acellular nerves was compared to that of the normal nerve (Fig. 2A-B). Normal nerves show a distinct perineurium with a myelin sheath and axonal structures. However, on microscopic observation of the acellular nerve, the axon and myelin structures disappeared, and only loose basal lamina tubes remained. Notably, there were no visible cells in the oriented ducts of the acellular nerve, and the pore size was significantly larger than that of the normal nerve, indicating that this superior acellular nerve fiber skeleton as a carrier of the drug delivery system may contribute to drug or cell loading and retention. The morphology of chitosan was observed using SEM. As presented in Fig. 2C, chitosan presented as a pipe shape with smooth surface, uniform thickness and texture.

Hematoxylin and eosin (HE) and immunofluorescence staining were applied to observe the composition, structure and ECM of acellular nerve. Longitudinal sections of the sciatic nerve were obtained (Fig. 2D). Compared to normal nerve fibers, which were dense and orderly, the acellular nerve fibers were loose and porous, and no cells were observed. We evaluated ECM retention by immunofluorescence staining of laminin (LN) and fibronectin (FN) in the acellular nerve. Many cells were observed in the longitudinal section of the normal nerve in the presence of LN and FN. The signal intensity of the acellular nerve was slightly lower than that of the normal nerve; however, the overall ECM was well preserved.

Live/dead staining of ADSCs with acellular nerves

To observe whether the acellular nerves prepared in this study were toxic to cells, ADSC-compounded acellular-MTs were cultured and stained with live/dead staining at

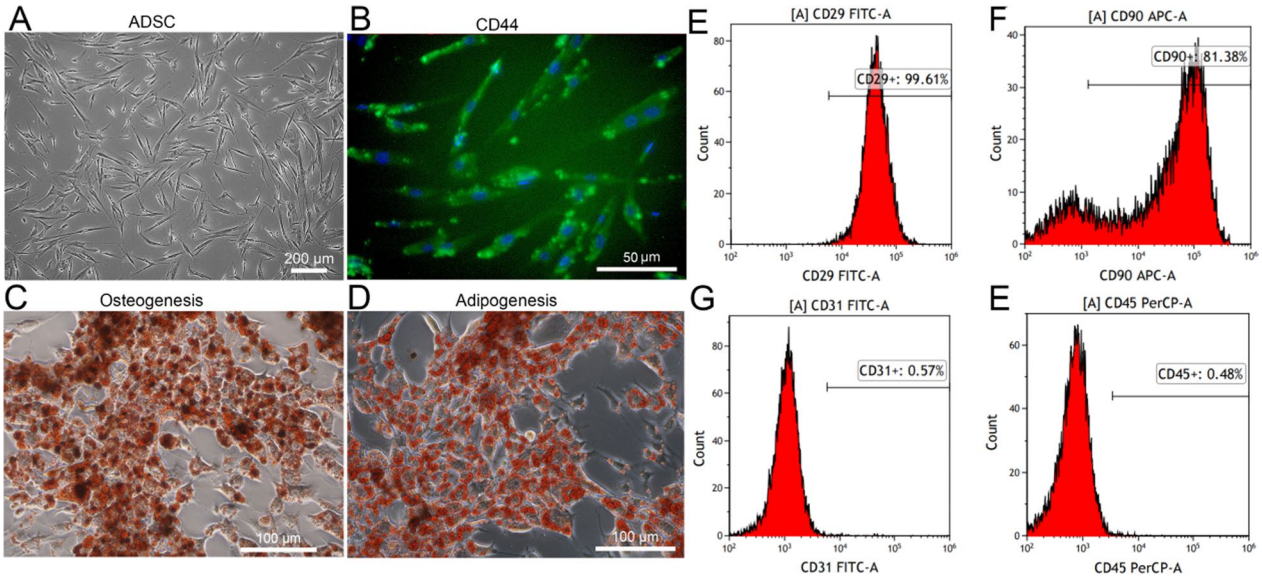

Fig. 1 Identification of ADSC. **A–D** Morphology of ADSC. ADSC exhibited multi-potential differentiation capacity for osteogenesis and adipogenesis. Scale bar: 50 μm, 100 μm, 200 μm. **E–H** Flow cytometric analysis of cell surface markers of ADSC

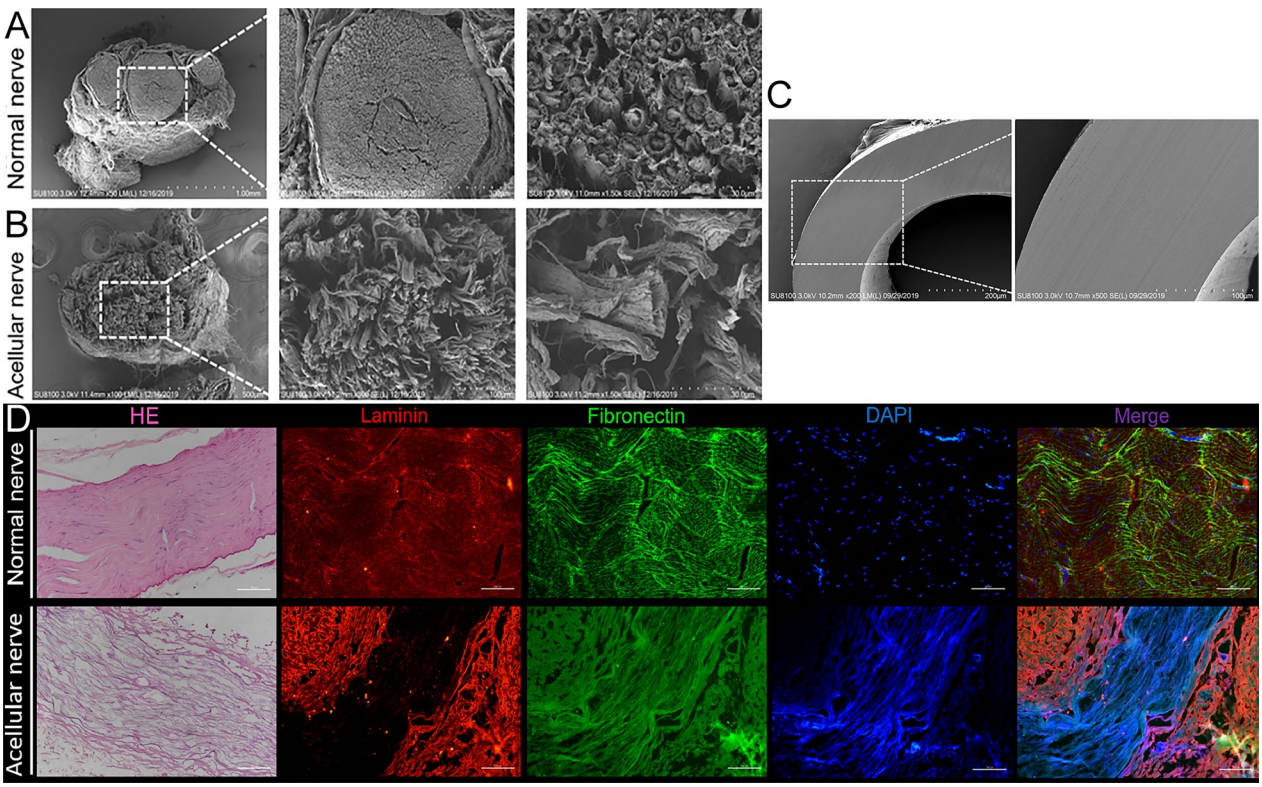

Fig. 2 Morphological observation of normal nerve, acellular nerve and chitosan. **A**–**B** SEM morphology of normal and acellular nerve. Normal nerves have a compact and ordered structure, while acellular nerves maintain a complete three-dimensional structure. **C** SEM morphology of chitosan. **D** HE staining and immunofluorescence staining of the laminin and fibronectin in normal nerve and acellular nerve. Scale bar: 100 μm

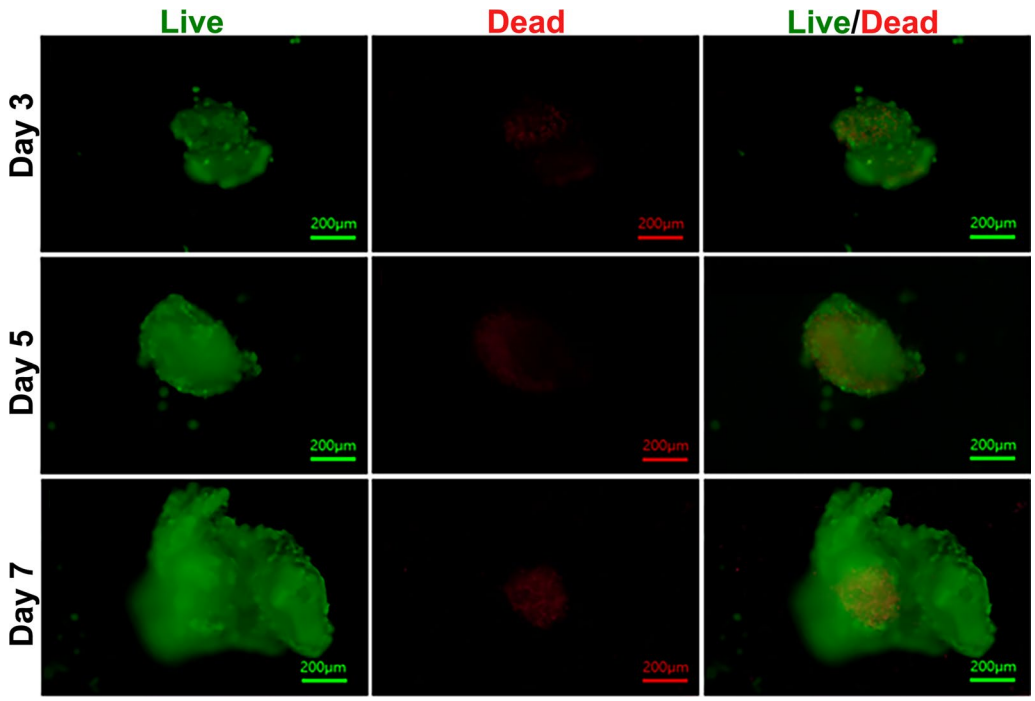

Fig. 3 Dead/alive staining of acellular nerve microtissue. FDA/PI bichromatic fuorescence staining was performed at 3d, 5d and 7d of ADSC coculture with acellular-MT. Green fluorescence denotes living cells and red fluorescence denotes dead cells. Scale bar: 200 μm

3-, 5-, and 7-days (d) (Fig. 3). After 7 d of culture, a large number of ADSCs proliferated, but the number of dead cells increased slowly, indicating that acellular-MT had good biocompatibility, was conducive to cell proliferation, and provided a good cell culture environment.

Evaluation of the functional recovery

To evaluate the functional recovery of acellular MTs combined with ADSCs in peripheral nerve defects in rats, the four experimental groups were compared. The walking trajectories of each group at 12 W post-operatively are shown (Fig. 4A), while the degree of functional recovery promoted by different treatment modalities was evaluated by plotting the intensity of the bilateral footprints in each group (Fig. 4B).

To further understand the therapeutic effect of the Acellular-MT + ADSC group, electrophysiological tests were conducted to evaluate whether functional recovery of peripheral nerve defects in rats was mediated by nerve grafts. The peak amplitude of the compound muscle action potential in each group at 12 W postoperatively was recorded and analyzed. At 12 W postoperatively, the CMAP amplitude and latency of the Chitosan + Acellular-MT + ADSC group were significantly improved compared with those of the chitosan and Chitosan + Acellular-MT groups. The action potential waveforms of the Chitosan + Acellular-MT + ADSC group were similar to those of the autograft group, indicating good recovery after peripheral nerve defect injury (Fig. 4C).

We subsequently compared the SFI of the Chitosan + Acellular-MT + ADSC group with those of the chitosan, Chitosan + Acellular-MT, and autograft groups to assess motor function recovery. The normal SFI of each rat before the operation was 0. Following establishment of the sciatic nerve defect model, the SFI values of the four groups decreased significantly, indicating a loss of sciatic nerve function. The SFI values were recorded and calculated at 4-, 8-, and 12-W postoperatively. At 4 W, each group showed a slight degree of functional recovery. Compared with the chitosan and Chitosan + Acellular-MT groups, the SFI values of the Chitosan + Acellular-MT + ADSC group gradually increased, but showed no significant difference from those of the autograft group ($^{**}p < 0.01$, $^{***}p < 0.001$, n = 5). At 8 and 12 W, the Chitosan + Acellular-MT + ADSC group showed a trend towards good sciatic nerve functional recovery, second only to the autograft group, which was significantly better than the chitosan and Chitosan + Acellular-MT groups, indicating that the Chitosan + Acellular-MT + ADSC group had a therapeutic level close to that of the autograft group (Fig. 4D).

The stand/swing time Ratio at 4-, 8-, and 12-W postoperatively were calculated to further evaluate the

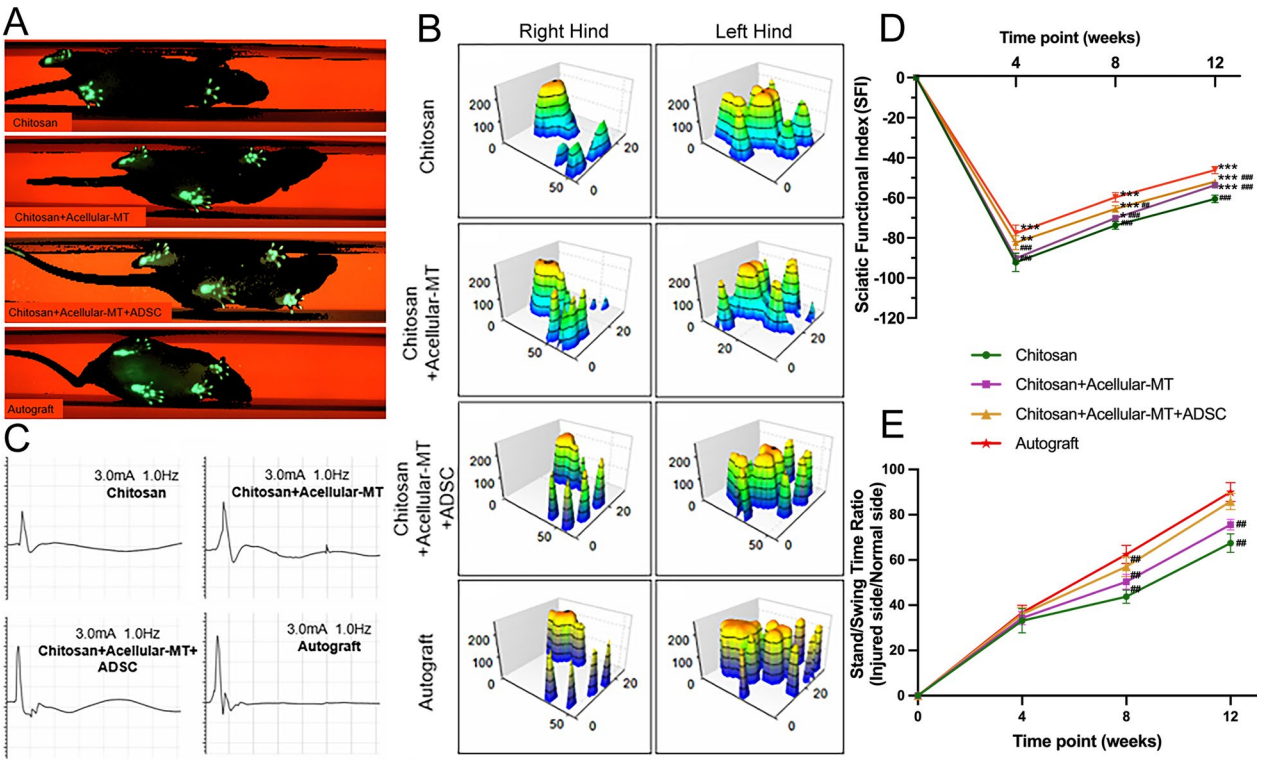

Fig. 4 Evaluation of neurological function recovery in each group. **A**–**B** Gait analysis and footprint strength analysis of 12W groups. **C** Electrophysiological recovery was assessed in each group at 12W, and CAMP on the operating side was recorded in each group. **D**–**E** SFI and Stand/Swing Time Ratio in 4W, 8W, 12W groups (*$P < 0.05$, **$P < 0.01$, ***$P < 0.001$,n = 5), vs. Chitosan group($^{\#\#}P < 0.01$, $^{\#\#\#}P < 0.001$, n = 5), vs. Autograft groups. Data are represented as mean ± SD

functional recovery of the injured side of the sciatic nerve. The data showed a trend similar to that of SFI. At 12 W postoperatively, the Stand/Swing Time Ratio of Chitosan + Acellular-MT + ADSC and autograft groups showed no significant difference, and was significantly better than those of the other two groups. This indicated that the Chitosan + Acellular-MT + ADSC group achieved efficacy similar to that of the autograft group (Fig. 4E).

Acellular-MT promotes axonal regeneration in sciatic nerve grafts

The effect of different treatments on sciatic nerve regeneration was evaluated by SEM analysis of the distal ends of the grafts 12 W postoperatively. The results showed that the myelinated nerve fibers in all grafts overgrew and reached the distal end of the graft segment. The autograft and Chitosan + Acellular-MT + ADSC groups had similar myelinated nerve fiber regeneration, and a more complete neural structure was observed, which was better than that in the chitosan and acellular-MT groups. The Chitosan + Acellular-MT + ADSC group further showed complete myelin formation, smoothness, good continuity, and nerve fibers with a wide diameter (Fig. 5A).

To further evaluate the regenerative nerve recovery in all groups, we measured the mean diameter and thickness of myelinated nerve fibers distal to the graft. The results showed that all parameters of the Chitosan + Acellular-MT + ADSC group were significantly higher than those of the chitosan group, while the mean diameters of the myelinated nerve and myelin sheath thickness were similar to those of the autograft group (Fig. 5B–C). In conclusion, our constructed acellular MT system could induce greater and better regeneration of myelin, which is similar to the gold standard for the treatment of peripheral nerve defects.

Longitudinal sections of grafts at 2 W postoperatively were stained with HE to observe the efficiency of the different treatment groups in promoting myelinated nerve regeneration. Obvious axonal ingrowth in the graft, which manifested as thicker myelin with better continuity, was observed in the Chitosan + Acellular-MT + ADSC group. We further observed a new axon extension in the Chitosan + Acellular-MT group, although the regeneration effect was significantly weaker than that of the acellular-MT composite ADSC (Fig. 6). The evaluation results were also encouraging. Our study confirmed that ADSCs based on acellular

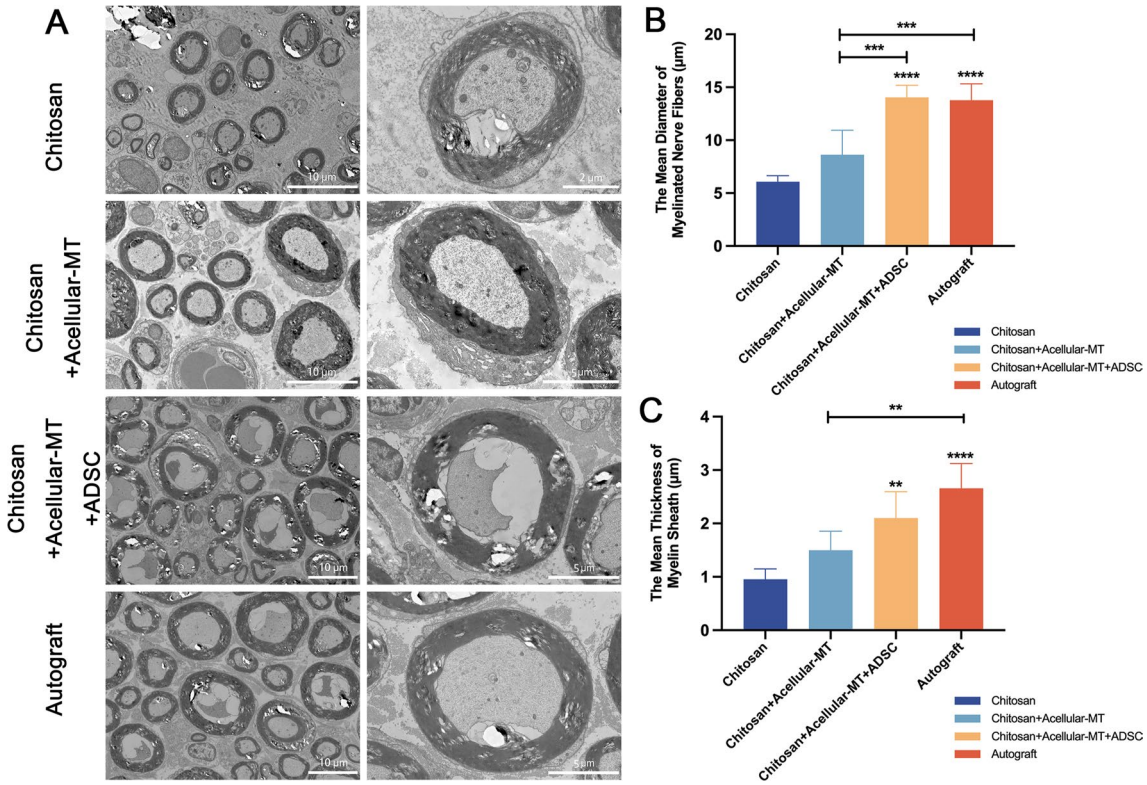

Fig. 5 The distal nerve graft was evaluated by SEM at 12W and analyzed statistically. **A** Representative images of the transverse section of myelinated nerve fibers in each group. **B** Calculate the mean diameter of myelinated nerve fibers. **C** Calculate myelin sheath thickness. (***P* < 0.01, ****P* < 0.001, *****P* < 0.0001, n = 5). Data are represented as mean ± SD

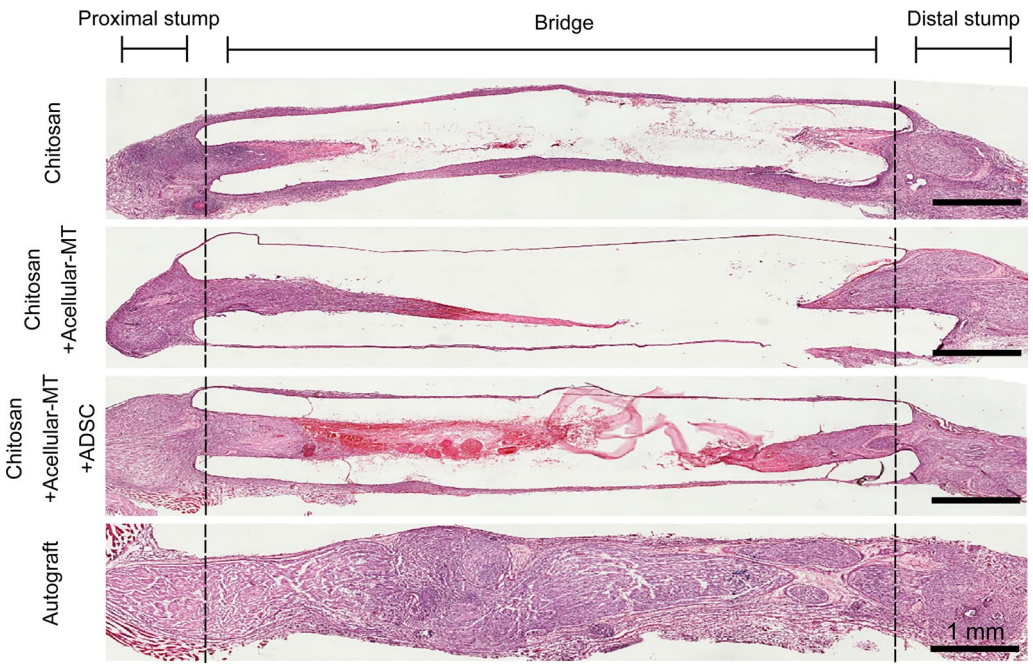

Fig. 6 HE staining was performed on the longitudinal section of nerve graft in each group at 2W. Axons are seen regenerating and growing into the nerve graft. Scale bar: 1 mm

allogeneic nerve-MT exhibited an excellent axonal regeneration rate at the early stage of transplantation, and could induce high-quality myelinated nerve fibers similar to the autograft group.

Acellular-MTs pre-recellularized with ADSCs accelerate vascular endothelial regeneration after sciatic nerve defect

To evaluate the extension of regenerated axons in the rat model of the 10 mm sciatic nerve defect, myelin regeneration and vascular endothelial reconstruction within the nerve graft were observed at 4d and 6d (Fig. 7). Nerve grafts from each group were sliced lengthwise and stained with anti-S100 and anti-RECA-1 antibodies. Red fluorescence extended and almost passed through the nerve graft segment on day 4 in the Chitosan + acellular MT + ADSC group. This showed a more obvious speed of vascular endothelial reconstruction, which is favorable for axon regeneration. The red and green fluorescence intensities of the Chitosan + AcellularMT + ADSC group were brighter at 6d than those in the Chitosan group, indicating that acellular nerve-MT could accelerate early angiogenesis and myelin regeneration.

Discussion

Peripheral nerve injury is a common clinical disorder that commonly results in motor dysfunction and loss of sensory function, resulting in long-term impacts on patient quality-of-life [11]. Prompt and effective treatment after injury is necessary to promote functional recovery [22]. The results of the present study showed that transplantation of allogeneic acellular microtissue pre-cellularized with ADSCs into a chitosan-constructed 3D culture platform to bridge the 10 mm gap in rats could enhance the regenerative repair of peripheral nerves [3, 23].

Selecting an appropriate nerve graft can further improve the efficacy of the surgical repair of nerve defects in clinical settings. Autografts are widely recognized as the "gold standard" for the treatment of severe nerve defects [24, 25]. However, there are many limitations to obtaining autologous nerves, including difficulty in obtaining a suitably sized and functional graft from the patient, intolerable neuroma, and increased operation time [26–28]. As such, it is necessary to develop new biomaterials to make up for the defects of autologous nerve transplantation [29, 30]. As an alternative to autografts, ANAs have been widely recognized as suitable materials for bridging nerve defects. Previous studies have revealed that motor nerve-derived grafts have a better effect at

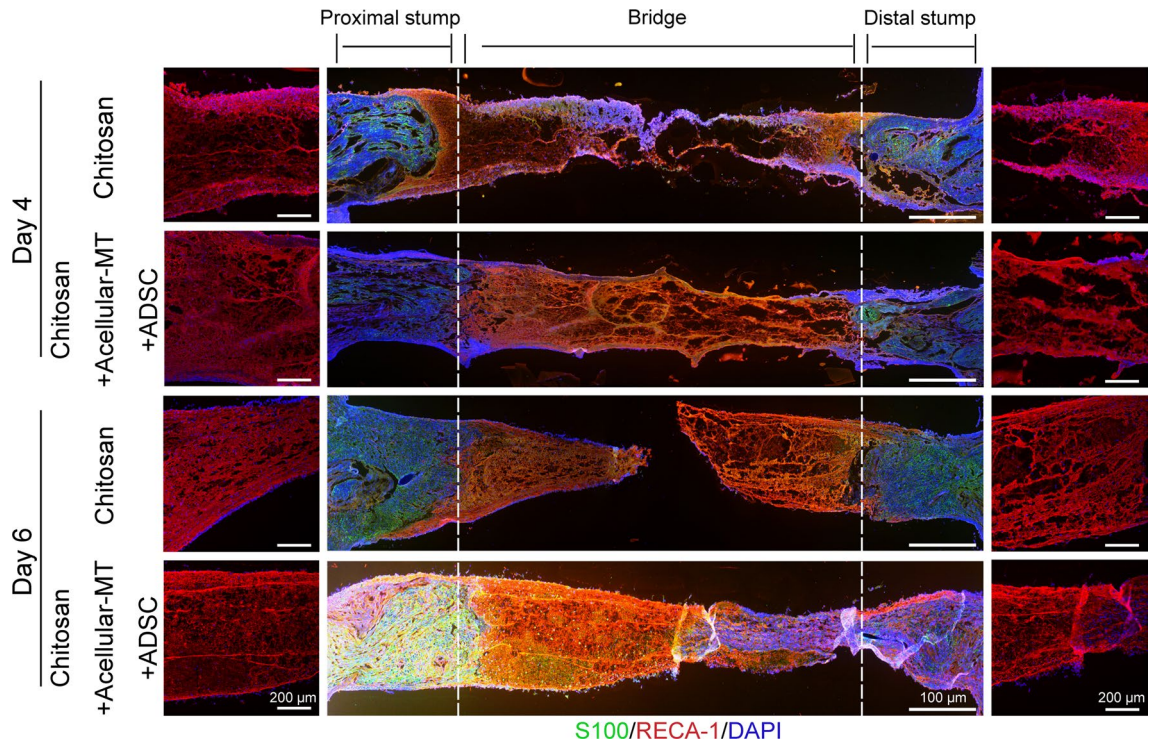

Fig. 7 The longitudinal sections of nerve grafts were stained with immunofluorescence at 4d and 6d. The regenerated myelin sheath was stained with anti-S100 antibody (green), and the regenerated vascular endothelium was stained with anti-endothelial Cell-1 antibody (red), the nucleus was stained with DAPI (blue). Scale bar: 100 μm, 200 μm

promoting axon regeneration and myelin formation than sensory nerve-derived grafts [2, 29, 31]. Therefore, we used rat sciatic nerves to prepare an acellular nerve scaffold. The main components of acellular nerves, the extracellular matrix (ECM), and internal microstructure are key to recruiting Schwann cells, which tend to migrate and induce myelinated nerve regeneration [9, 32]. Cell growth and culture are complex processes that require the co-regulation of several glycoproteins [6, 17]. The composition of the ECM, as an effective "soil" for cell growth, is primarily determined by its abundant glycoproteins [9, 33]. LN, together with collagen, forms the basement membrane; its primary biological function is to promote cell adhesion to the matrix and to regulate cell growth and differentiation [27, 28]. As an important ECM component, FN have various biological functions [34]. The most important of which is to promote adhesion and growth between cells, as effective adhesion of cells can promote injury healing and exert biological functions [35]. The two-step procedural decellularization method developed by Sondell et al. has been proven to maintain relatively rich ECM components and a complete microstructure [7, 10] that is close to the endogenous environment of cell growth [36]. However, the detergent control remains problematic [24]. Excessive chemical processes are used to remove immunogenicity from the pores to a greater extent in the traditional decellularization process, resulting in the destruction of ECM components of ANA, such as laminin, collagen, and bioactive factor [13]. Excessive detergent can also come into contact with the ANA nerve stump, which was not conducive to anastomosis and repair of the graft and nerve stump [2, 30, 37]. However, to retain an abundant ECM, it is necessary to reduce the amount of detergent required [31, 34, 35]. Although the decellularization process can almost completely remove the cellular components that induce autoimmune reactions, some substances will inevitably remain, leading to hidden dangers when using the decellularized nerve as a nerve defect bridging the graft [1, 23, 33, 38].

In addition to the effect of the degree of decellularization, the dense internal structure of the acellular nerve graft limits the growth of regenerated axons at the severed end of the nerve into this segment [13, 21, 22]. Under physiological conditions, normal nerves have low porosity, a small pore size, and a dense structure, while the wrapping of axons and myelin in basal tubes is conducive to maintaining their growth and physiological roles [11, 39–41]. During the repair process of injured nerves, Schwann cells migrate into the graft, release neurotrophic factors, and form Büngner bands, which induce the extension of regenerated axons [7, 9, 10, 36, 42, 43]. However, the original structure of traditional acellular nerves is dense, which is not conducive to the growth and extension of regenerative myelinated nerves [8, 18, 44, 45].

It is worth noting that the use of acellular scaffolds could avoid these problems [6]. Indeed, microtissue engineering has been used to develop acellular scaffolds as carriers for regenerative medicine [8]. The overarching goal is to construct an acellular nerve with low immunogenicity and ECM integrity that allows for a large number of cells to survive and perform their repair functions [6]. Acellular scaffolds have a loose structure, which is more conducive to endogenous Schwann cell infiltration during nerve dissection, and promotes nerve regeneration [29, 32]. To achieve this structure, we obtained the motor nerves of allogeneic species and prepared them into 1 mm diameter microparticles [9, 30]. Acellular microparticles were subsequently obtained by traditional decellularization neurochemical processes and decellularization was performed using an appropriate detergent [12, 19, 20]. Owing to the small diameter of the prepared microparticles, full contact with the stain remover resulted in a high degree of decellularization, while the ECM and other components favorable for cell growth were retained to the greatest extent [6, 17].

ADSCs have good regenerative and secretory abilities, and can be targeted to deliver stimulants related to nerve regeneration, such as neurotrophic factors, soluble factors, and cytokines [35, 36]. The levels of many biological factors at the injured site were increased to provide the optimal environmental conditions for tissue regeneration [25, 27, 30]. The recruitment of endogenous Schwann cells to injured sites can accelerate the extension of axons and play a positive role in repairing peripheral nerve defects [30, 32]. In addition, ADSCs can be obtained through a simple in vitro amplification method and are promising nerve regeneration cells for cell therapy [3, 15, 18]. Stem cell therapy can further compensate for the lack of endogenous Schwann cells in acellular MTs [19, 36, 38]. For acellular nerve grafts, sufficient autologous Schwann cells are required to infiltrate the nerve ends and promote the growth of regenerated nerves throughout the defect [32, 40]. The repair process is believed to be slow because of the insufficient driving effect of Schwann cells [4, 5]. This process involves the infiltration, expansion, and arrangement of Schwann cells [32]. The acellular neural bridge strategy also does not apply to the treatment of long-segment defects (>3 cm), as Schwann cells cannot complete the graft [1, 41]. The failure of repair may result in an insufficient migration driving force and/or a short proliferation cycle of Schwann cells, which makes it difficult to meet the demands of transplanting segments [23, 25]. As such, microtissue engineering scaffolds have been used to promote the

proliferation and arrangement of Schwann cells in the graft, induce the formation of Büngner bands, and accelerate the axon regeneration rate [28, 29]. Using acellular nerve particles as neural scaffolds, supporting cells were cultured on neural scaffolds to modify the ECM, while a three-dimensional culture environment suitable for cell growth was constructed [6, 9]. On the one hand, acellular-MT can accommodate more supporting cells, simulate the physical and chemical characteristics of natural ECM in vivo, and exert the positive effects of the ECM on the in situ environment [10, 39]. However, on the other hand, the neurotrophic factors secreted by the supporting cells contribute to the recruitment of endogenous Schwann cells that participate in myelinated nerve regeneration [11, 21]. This acellular MT, with a large pore size and low biotoxicity, is conducive to the extension of regenerative axons to the distal end of the graft, resulting in faster repair and regeneration quality [3, 23, 26].

Chitosan is one of the most popular scaffolds in tissue engineering due to its high biocompatibility, good tensile resistance, and biodegradability [12, 39]. There have been many studies investigating the utility of chitosan as a natural biological scaffold to repair damaged peripheral nerves using combined cell or factor therapy, such as chitosan combined with fibroin filaments to construct a good regenerative peripheral nerve scaffold, which has achieved good curative effects in the treatment of peripheral nerve defects in rats [9, 16, 29, 41]. This prior research helped us to develop the encapsulation vector of Acellular-MT.

In the present study, we filled chitosan with acellular nerve microparticles combined with ADSC to construct MT and bridge a 1 cm nerve defect of peripheral nerves in rats to explore the ability of MT to promote peripheral nerve regeneration and repair. Our results showed that no cellular components were present in the acellular MTs, and that the fibers were loose and porous. Immunofluorescence staining revealed that the main bioactive components of the ECM, glycoproteins including LN and FN, remained intact, which is considered to be key for the acellular-MT to help cells perform the repair function and promote axon regeneration and extension. After 7 days, Schwann cells were co-cultured with acellular-MT, showing good survival and proliferation, indicating that the constructed acellular-MT had good biocompatibility. To evaluate the degree of recovery of nerve function after the repair of peripheral nerve defects with acellular-MT, we analyzed the sciatic nerve SFI value and the stand/swing time ratio of each group, finding that the Chitosan + Acellular-MT + ADSC group showed a recovery advantage second only to the autograft group at 8 W postoperatively, while the degree of recovery showed no significant difference with the autograft group at 12 W postoperatively. The electrophysiological characteristics of the nerves were similar to those of the autograft group, which also reflected a strong ability to promote the regeneration of peripheral nerve defects. SEM analysis of the distal nerve grafts at 12 W after the operation in each group and the effect on sciatic nerve regeneration were evaluated, revealing that the structure of myelinated nerve fibers in the Acellular-MT group showed good continuity of the regenerative myelin sheath, smooth shape, and wider diameter of nerve fibers, similar to that in the autograft group.

Conclusion

In conclusion, the present study showed that our constructed acellular-MT combined with ADSCs provided a nutrient-rich three-dimensional culture environment to provide better support to cells, allowing them to play a reparative role in the graft segment, accelerate the growth of regenerated axons at the broken nerve end, and extend to the distal end of the graft. This indicates that microtissue composite stem cell therapy may provide good support for the application of acellular scaffolds in regenerative medicine.

Abbreviations

ADSC	Adipose mesenchymal stem cells
MT	Microtissue
ANA	Acellular nerve allografts
ECM	Extracellular matrix
FDA	Fluorescein diacetate
PI	Propidium iodide
SFI	Sciatic nerve function index
PL	Print length
TS	Toe spread
IT	Intermediary toe spread
CMAPs	Compound muscle action potentials
HE	Hematoxylin and eosin
LN	Laminin
FN	Fibronectin
SEM	Scanning electron microscope

Supplementary Information

The online version contains supplementary material available at https://doi.org/10.1186/s13287-024-04093-5.

Additional file 1.

Acknowledgements

The authors declare that they have not use AI-generated work in this manuscript.

Author contributions

ZZF: data curation, investigation, project administration, supervision, writing—review & editing. LML: conceptualization, investigation, resources, validation, writing—original draft. CG: data curation, project administration, writing—original draft. WP: methodology, validation, writing—original draft. ZCH: investigation, software, writing—original draft. LY: formal analysis, methodology, writing—original draft. DXF: data curation, formal analysis, writing—original draft. WJ: supervision, writing—review & editing. JYJ: formal analysis. XF: conceptualization, visualization, writing—review & editing. ZYQ:

methodology, supervision, writing—review & editing. ZJN: conceptualization, resources, supervision, writing—review & editing.

Funding
This study was supported by the grants from China Postdoctoral Science Foundation, NO. 2021MD703963. This study was supported by the grants from the National Natural Science Foundation of China, NO. 82102079.

Availability of data and materials
Data availability is not applicable to this article as no new data were created or analyzed in this study.All data in this research study are available from the corresponding author upon reasonable request.

Declarations

Ethics approval and consent to participate
Title of the approved project: Nerve defect animal model(SD rats). Name of the institutional approval committee: the Ethics Committee of the Chinese PLA General Hospital. Approval number: SQ2022437. Date of approval: 2022-04-03. (2)Title of the approved project: Preparation of acellular nerves(SD rats). Name of the institutional approval committee: the Ethics Committee of the Chinese PLA General Hospital. Approval number:2022-X18-37. Date of approval:2022-01-08. In this study, all animal experiments were carried out following the guidelines and regulations related to the care and use of laboratory animals presented by the animal ethics committee of the Chinese PLA General Hospital (Code No.2022-X18-37).

Consent for publication
Not applicable.

Competing interests
The authors declare no competing interests.

Author details
[1]Departments of Neurosurgery, The First Center of Chinese, PLA General Hospital, Beijing, China. [2]Departments of Ultrasound, Tianjin Medical University Cancer Institute & Hospital, Tianjin, China. [3]Departments of Ultrasound, The First Center of Chinese, PLA General Hospital, Beijing, China. [4]Departments of Neurosurgery, Chinese PLA General Hospital, Beijing, China. [5]Department of Urology, The Affiliated Hospital of Changchun University of Chinese Medicine, Changchun, Jilin, China. [6]Department of Anesthesiology, Beijing Chao-Yang Hospital, Capital Medical University, Beijing, China. [7]Department of Orthopedic, Maanshan General Hospital of Ranger-Duree Healthcare, Maanshan, Anhui, China.

Received: 21 August 2024 Accepted: 4 December 2024
Published online: 31 December 2024

References

1. Kong L, et al. Multilevel neurium-mimetic individualized graft via additive manufacturing for efficient tissue repair. Nat Commun. 2024;15(1):6428.
2. Wang J-Y, et al. Remodeling of the intra-conduit inflammatory microenvironment to improve peripheral nerve regeneration with a neuromechanical matching protein-based conduit. Adv Sci (Weinheim, Baden-Wurttemberg, Germany). 2024;11(17): e2302988.
3. Zhang J, et al. A 3D-Printed Self-Adhesive Bandage with Drug Release for Peripheral Nerve Repair. Adv Sci (Weinheim, Baden-Wurttemberg, Germany). 2020;7(23):2002601.
4. Thomson SE, et al. Bioengineered nerve conduits and wraps for peripheral nerve repair of the upper limb. Cochrane Database Syst Rev. 2022;12(12):CD012574.
5. Li X, et al. Biological characteristics of tissue engineered-nerve grafts enhancing peripheral nerve regeneration. Stem Cell Res Ther. 2024;15(1):215.
6. Wang S, et al. BMSC-derived extracellular matrix better optimizes the microenvironment to support nerve regeneration. Biomaterials. 2022;280: 121251.
7. El Soury M, et al. Comparison of decellularization protocols to generate peripheral nerve grafts: a study on rat sciatic nerves. Int J Mol Sci. 2021;22(5):2389.
8. Han S, et al. Chiral hydrogel nerve conduit boosts peripheral nerve regeneration via regulation of Schwann cell reprogramming. ACS Nano. 2024;18(41):28358–70.
9. Zhang X, et al. Decellularized extracellular matrix scaffolds: recent trends and emerging strategies in tissue engineering. Bioact Mater. 2022;10:15–31.
10. Sun X, et al. Devising micro/nano-architectures in multi-channel nerve conduits towards a pro-regenerative matrix for the repair of spinal cord injury. Acta Biomater. 2019;86:194–206.
11. Kwon J, et al. Engineered regenerative isolated peripheral nerve interface for targeted reinnervation. Adv Mater (Deerfield Beach, Fla). 2024;36(44): e2406652.
12. Xing H, et al. Extracellular matrix-derived biomaterials in engineering cell function. Biotechnol Adv. 2020;42: 107421.
13. Liu Z, et al. Hyaluronic acid extracellularly inhibits ferroptosis via cell-surface receptors in acute traumatic brain injury. Nano Today. 2022;46: 101625.
14. Song M, et al. Amplified targeted drug delivery independent of target number through alternative administration of two matched nanoparticles. ACS Nano. 2023;17(23):23359–73.
15. Yang Z, et al. Applications of induced pluripotent stem cell-derived glia in brain disease research and treatment. Handb Exp Pharmacol. 2023;281:103–40.
16. Sun, Z., et al., *Bioactive Peptide Hydrogel Scaffold with High Fluidity, Thermosensitivity, and Neurotropism in 3D Spatial Structure for Promoted Repair of Spinal Cord Injury.* Small, 2024: p. e2406990.
17. Li G, et al. Bionic microenvironment-inspired synergistic effect of anisotropic micro-nanocomposite topology and biology cues on peripheral nerve regeneration. Sci Adv. 2021;7(28): eabi5812.
18. Tan F, et al. Clinical applications of stem cell-derived exosomes. Signal Transduct Target Ther. 2024;9(1):17.
19. Putthanbut N, Lee JY, Borlongan CV. Extracellular vesicle therapy in neurological disorders. J Biomed Sci. 2024;31(1):85.
20. Zhao F, et al. Extracellular vesicles from Zika virus-infected cells display viral E protein that binds ZIKV-neutralizing antibodies to prevent infection enhancement. EMBO J. 2023;42(6): e112096.
21. Nie X, et al. Full-scale osteochondral regeneration by sole graft of tissue-engineered hyaline cartilage without co-engraftment of subchondral bone substitute. Adv Healthcare Mater. 2020;9(2): e1901304.
22 Wang L, et al. A fully biodegradable and self-electrified device for neuroregenerative medicine. Sci Adv. 2020;6(50): eabc6686.
23. Chen A, et al. Multimaterial 3D and 4D bioprinting of heterogenous constructs for tissue engineering. Adv Mater (Deerfield Beach, Fla). 2024;36(34): e2307686.
24 Xu D, et al. Ultrasound-Responsive Aligned Piezoelectric Nanofibers Derived Hydrogel Conduits for Peripheral Nerve Regeneration. Adv Mater (Deerfield Beach, Fla). 2024;36(28): e2307896.
25. Smith DH, et al. Tissue-engineered grafts exploit axon-facilitated axon regeneration and pathway protection to enable recovery after 5-cm nerve defects in pigs. Sci Adv. 2022;8(44): eabm3291.
26 Lan L, et al. Sustainable natural bio-origin materials for future flexible devices. Adv Sci (Weinheim, Baden-Wurttemberg, Germany). 2022;9(15): e2200560.
27. Kornfeld T, et al. Spider silk nerve graft promotes axonal regeneration on long distance nerve defect in a sheep model. Biomaterials. 2021;271: 120692.
28. Wang W, et al. Skin organoid transplantation promotes tissue repair with scarless in frostbite. Protein Cell. 2024;pwae055.
29 Jin Y, et al. Scaffold-based tissue engineering strategies for urethral repair and reconstruction. Biofabrication. 2024;17(1):012003.
30. Murphy PL, Isaacman-Beck J, Granato M. Robo2 drives target-selective peripheral nerve regeneration in response to glia-derived signals. J Neurosci Off J Soc Neurosci. 2022;42(5):762–76.
31. Duan X, et al. Piezoelectrically-activated antibacterial catheter for prevention of urinary tract infections in an on-demand manner. Mater Today Bio. 2024;26: 101089.

32. Fuentes-Flores A, et al. Senescent Schwann cells induced by aging and chronic denervation impair axonal regeneration following peripheral nerve injury. EMBO Mol Med. 2023;15(12): e17907.
33. Zhang Y, et al. Mouse circulating extracellular vesicles contain virus-derived siRNAs active in antiviral immunity. EMBO J. 2022;41(11): e109902.
34. Zheng C, et al. Nanofibrous nerve guidance conduits decorated with decellularized matrix hydrogel facilitate peripheral nerve injury repair. Theranostics. 2021;11(6):2917–31.
35. Lewis M, et al. Neuro-regenerative behavior of adipose-derived stem cells in aligned collagen I hydrogels. Mater Today Bio. 2023;22: 100762.
36. Zhou LN, et al. A comparison of the use of adipose-derived and bone marrow-derived stem cells for peripheral nerve regeneration in vitro and in vivo. Stem Cell Res Ther. 2020;11(1):153.
37. Tang Y, et al. Platelet extracellular vesicles enhance the proangiogenic potential of adipose-derived stem cells in vivo and in vitro. Stem Cell Res Ther. 2021;12(1):497.
38. Saffari S, et al. Mesenchymal stem cells and local tacrolimus delivery synergistically enhance neurite extension. Biotechnol Bioeng. 2021;118(11):4477–87.
39 Cho Y, et al. Emerging materials and technologies with applications in flexible neural implants: a comprehensive review of current issues with neural devices. Adv Mater (Deerfield Beach, Fla). 2021;33(47): e2005786.
40. Yang Z, et al. Engrafted glial progenitor cells yield long-term integration and sensory improvement in aged mice. Stem Cell Res Ther. 2022;13(1):285.
41. Chen T, et al. Essential elements for spatiotemporal delivery of growth factors within bio-scaffolds: a comprehensive strategy for enhanced tissue regeneration. J Controll Release Off J Controll Release Soc. 2024;368:97–114.
42. Kaplan HM, Mishra P, Kohn J. The overwhelming use of rat models in nerve regeneration research may compromise designs of nerve guidance conduits for humans. J Mater Sci Mater Med. 2015;26(8):226.
43. Fu X, et al. Induction of adipose-derived stem cells into Schwann-like cells and observation of Schwann-like cell proliferation. Mol Med Rep. 2016;14(2):1187–93.
44. Ding X, et al. Cobweb-inspired microenvironment-targeting nanosystem with sequential multiple-stage stimulus-response capacity for ischaemic tissue repair. Adv Func Mater. 2023;33(32):2301451.
45. Kim B-S, et al. Comparative analysis of supercritical fluid-based and chemical-based decellularization techniques for nerve tissue regeneration. Biomater Sci. 2024;12(7):1847–63.

Publisher's Note